International Journal of Multiphase Flow 106 (2018) 138–146

Contents lists available at ScienceDirect

International Journal of Multiphase Flow

journal homepage: www.elsevier.com/locate/ijmulflow

The lifespan of clusters in confined bubbly liquids

B. Figueroa-Espinoza[a], B. Mena[b], A. Aguilar-Corona[c], R. Zenit[d,*]

[a] Laboratorio de Ingeniería y Procesos Costeros, Instituto de Ingeniería, Universidad Nacional Autónoma de México, Sisal, Yucatán 97835, Mexico
[b] Instituto de Ingeniería, Universidad Nacional Autónoma de México, Ciudad de México 04510, Mexico
[c] Facultad de Ingeniería Mecánica, Universidad Michoacana de San Nicolás de Hidalgo, Morelia, Michoacán 58030, Mexico
[d] Instituto de Investigaciones en Materiales, Universidad Nacional Autónoma de México, Ciudad de México 04510, Mexico

ARTICLE INFO

Article history:
Received 8 November 2017
Revised 16 May 2018
Accepted 17 May 2018
Available online 18 May 2018

Keywords:
Clusters lifespan
Clustering
Bubbly flow
Velocity fluctuations

ABSTRACT

A nearly monodispersed bubbly flow in a Hele–Shaw type channel was studied, for large but finite Reynolds numbers. Experiments were carried out with millimetre-sized Nitrogen bubbles rising through water-glycerin mixtures.The velocities, geometry and other flow characteristics were measured by means of a high speed camera and an image processing routine, in order to validate this experimental set-up with previous results from the literature and shed some light on the cluster formation, timespan and breakup mechanisms. The timespan of clusters was estimated by tracing the clusters trajectories. The results show that clustering occurs, but the bubble aggregates breakup rapidly due to hydrodynamic effects. Scaling arguments were used to obtain an estimate for the lifespan, which is compared to experiments. This estimate does not take into account wake effects, so it can be interpreted as a lower bound of clusters lifespan in an homogeneous bubbly flow.

1. Introduction

If anyone observes a single millimetric air bubble rising through quiescent water, one notices that its trajectory is a straight line (for bubbles of diameter smaller than one millimeter); however, if a pair of such bubbles rise close to each other, their trajectories follow complicated paths, due to the hydrodynamic interaction between bubbles and the (initially still) liquid. The case where inertial forces dominate over viscous can be characterized by a large Reynolds number *Re*, defined as

$$Re = \frac{u_b D_{eq} \rho}{\mu} \tag{1}$$

where D_{eq} is the bubble equivalent diameter and u_b is the average bubble rise velocity, ρ and μ are the liquid density and viscosity, respectively. If surface tension forces are also small compared to inertial terms, the Weber number is small. This number is defined by

$$We = \frac{\rho u_b^2 D_{eq}}{\sigma} \tag{2}$$

where σ is the surface tension. For the dual limit of large Reynolds and small Weber numbers, potential flow theory can be used to study hydrodynamic interactions; Biesheuvel and Van Wijngaarden (1982), Kok (1989), Kumaran and Koch (1993a,b) analyzed the motion of two bubbles ascending in quiescent liquid and carried out the calculation of the bubble trajectories, which were then compared with careful experiments in the laboratory. The actual trajectories were fairly well predicted by the theory, based on velocities calculated from a potential and a set of dynamical equations for the relative velocities and the center of mass of the two bubbles array. These trajectories are complex, but in general terms, the bubbles tend to come together and collide along the line perpendicular to gravity if their initial orientation is not close to a vertical alignment between bubbles centers. One would expect, based on the aforementioned argument, that bubbles in an initially homogeneous bubbly flow would tend to form horizontally oriented clusters. This clustering phenomenon was also predicted by numerical simulations (Sangani and Didwania, 1993; Smereka, 1993), where potential flow hydrodynamic interactions between (many) bubbles lead to the formation of horizontal bubble clusters (in absence of coalescence).

In the case of a cloud of bubbles, the motion of other bubbles generates forces (that depend on the relative positions and velocities) on each test bubble. Moreover, these forces cause deformations on the bubbles surfaces, which are also coupled to the liquid. This interaction between the flow field, forces and deformations is hard, if not impossible to describe mathematically in a deterministic manner. This situation led (Van Wijngaarden, 1993) to treat the problem with stochastic tools, based on a set of simplified equa-

* Corresponding author.
E-mail address: zenit@unam.mx (R. Zenit).

https://doi.org/10.1016/j.ijmultiphaseflow.2018.05.012
0301-9322/

tions of motion for a pair of bubbles that resulted from the work of Kok (1989). These simplifications served the purpose of calculating an ensemble average for the liquid vertical velocity $\langle u_y \rangle$:

$$\langle u_y \rangle = u_b\{1 - 1.56\alpha + O(\alpha^2) + ...\} \tag{3}$$

where u_b is the terminal rise velocity of a free bubble and α is the gas volume fraction in the liquid-gas suspension. Eq. (3) states that at higher volume fractions the mean bubble velocity decreases. This result agrees with the actual qualitative behavior of bubble suspensions (Van Wijngaarden and Kapteijn, 1990; Clift et al., 1978; Zenit et al., 2001).

Because of linearity, binary hydrodynamic interactions can also be used to calculate properties and averaged equations for bubbly liquids, as was done by Spelt and Sangani (1998), who determined average properties in the limit of large Reynolds and small Weber numbers, as a function of the volume fraction, such as mean relative velocity and velocity variance of the bubbles, using numerical simulations and pair interaction theory. Kok (1993), also calculated the mean-square fluctuating velocity in a uniform suspension and the hydrodynamic diffusivities in a nonuniform one, by performing an ensemble average over pair interactions. This pair averaging procedure is valid for dilute suspensions ($\alpha \ll 18/Re$). These statistical techniques are a powerful tool for modeling complex systems like multiphase flows.

Experimental measurements of bubble clusters are difficult because of the superposition of bubbles when observing a bubble cloud, as well as the cluster breakup due to motion-induced agitation. Nevertheless, some observations of clustering have been reported in 3D experiments by Zenit et al. (2001) and Figueroa-Espinoza and Zenit (2005), the latter being able to obtain statistical evidence of horizontal clustering in a thin channel. The problem with the 2D viewpoint is that the wall effects are strong, and may themselves cause clustering, since when a bubble rises near a wall its velocity decreases and a transverse lift force tends to attract it towards the wall, causing it to bounce (Figueroa-Espinoza et al., 2008), blocking the trailing bubbles motion and (potentially) causing them to form clusters. A similar effect has been observed near a wall in the presence of surfactants (Takagi et al., 2009). Nevertheless, if one compares the radial distribution functions for the experiments in Figueroa-Espinoza and Zenit (2005) with those coming from 3D numerical simulations (Bunner and Tryggvason, 2002a), the qualitative agreement is reasonable.

Bubble clusters may cause the whole flow field to behave differently, with respect to a uniformly distributed suspension of bubbles. Clusters could influence the surrounding flow field (Salesse et al., 2002; Van Wijngaarden, 2005), introducing enhanced velocity fluctuations and hydrodynamic interactions that could affect the overall flow structure. The way clusters interact with the overall flow is not yet well understood, but the importance of certain flow parameters on their formation and dynamics has already been identified: the effect of the volume fraction, α, on the added mass coefficient was first theoretically calculated by Van Wijngaarden (1976) for uniformly distributed bubbly flows. Spelt and Sangani (1998) noted that the added mass coefficient for clustered bubbly liquids was much greater than the theoretical predictions for uniformly distributed bubbles. They also showed that the tendency to form aggregates is diminished when the velocity fluctuations in the bubbly liquids are increased. The formation of clusters was not observed for sufficiently low values of the bubbly turbulent intensity (the ratio between the magnitude of the mean relative velocity of the bubbles and their root-mean-squared velocity). If the bubble aggregates contribution to the velocity fluctuations is important, then they may contribute to their own breakup, so it would be reasonable to expect their lifespan to be very short. This was observed by Bunner and Tryggvason (2002a).

The reason for focusing our attention on velocity fluctuations are numerous: whenever an attempt is made to obtain averaged equations of motion for a bubbly flow, just as in the case of turbulent flows (Van Wijngaarden, 1997), some terms appear, (equivalent to the Reynolds stresses in turbulence models) which depend on velocity fluctuations. These terms are related to the transport of momentum due to fluctuations in the velocity of bubbles, collisions, and hydrodynamic interactions. Since these averaged equations are usually developed from the assumption that the velocity field is the sum of a deterministic part plus a stochastic part, the structure of the latter is of interest in many situations. There is a previous work which is closely related to our investigation: Zenit et al. (2001) measured the liquid and bubble velocities for a bubble monodispersed suspension using a dual impedance probe. They also calculated a first approximation for the liquid velocity variance, using the potential of a single bubble rising through a liquid at rest. By calculating the squared velocity disturbance on a single bubble, multiplying it by the number density and integrating over all the space, they obtained:

$$\langle u_x^2 \rangle = \frac{1}{5}\alpha u_b^2 \tag{4}$$

$$\langle u_y^2 \rangle = \frac{3}{20}\alpha u_b^2 \tag{5}$$

where u_b is the bubble velocity relative to the liquid for a given α. This calculation was first derived by in Biesheuvel and Van Wijngaarden (1984).

There are other attempts to evaluate the velocity fluctuations, in order to obtain more accurate estimates for the quantities involved in calculations for averaged equations. Van Wijngaarden (1997) also calculated expressions for the excess turbulent energy caused by the presence of the bubbles, and also found it to be dependent on αu_b^2. These quantities have units of energy, and are usually the only quantities that can be obtained in turbulence related experiments.

More recently, bubble-induced agitation motivated some experimental investigations (Martinez-Mercado et al., 2007; Mercado et al., 2013; Riboux et al., 2009) on the properties, scaling and interaction between the gas volume fraction, velocity PDF, liquid velocity fluctuations and observed energy spectrum, in order to shed some light on the origin of such enhanced fluctuations; Riboux et al. (2009) carried out an experiment with homogeneous bubbly flows with different bubble sizes and volume fractions, being able to obtain bubble mean velocity, liquid velocity fluctuations and Energy Spectrum using optical probes and Laser Doppler anemometry behind homogeneous bubble swarms. The velocity fluctuations (defined as the vertical velocity variance normalized with the single bubble terminal velocity $u_b(\alpha \to 0)$) resulted to scale as $\alpha^{0.8}$, where α is the gas volume fraction. The Energy Spectrum follows a power law in terms of the wavelength close to 3, consistent with other studies related to bubble induced turbulence (Lance and Bataille, 1991; Mendez et al., 2013). Interestingly, later numerical simulations (Riboux et al., 2008) , where the bubbles were modelled by fixed momentum forces of finite size randomly distributed in an uniform flow (for a volume fraction in the range $0.006 < \alpha < 0.04$), reproduced the velocity fluctuations and Energy Spectrum scaling of the experiments, suggesting that the wakes play a very important role in bubble-induced turbulence (Riboux et al., 2008). This set-up of fixed objects (a random distribution of spheres in a channel) immersed in a uniform flow was carried out experimentally by Risso et al. (2008); this configuration allowed for both temporal and spacial averaging, which showed that Large-Reynolds-number bubble-induced agitation was driven by (large scale) wake interactions. Interest in explaining theoretically the aforementioned scaling has motivated some new models

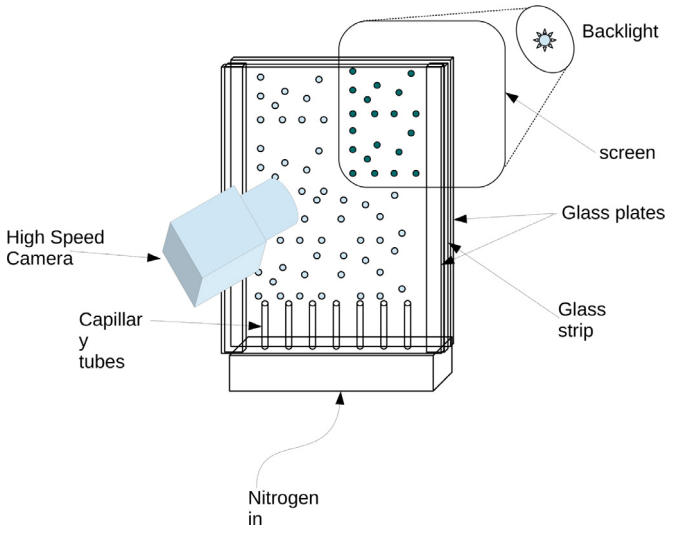

Fig. 1. Experimental setup. The thin channel was built with two glass plates separated by two glass strips. Nitrogen is injected through the capillary bank to produce the bubbles.

based on potential flow (Eames et al., 2004; Roig, 2007), as well as stochastic considerations (Risso, 2011, 2016). Of great importance is the recent review article by Risso (2018), where a summary of the 'state-of-the art' of the subject can be found.

The objective of this investigation is to contribute to the understanding of bubbly flow hydrodynamics, by comparing theory and experiments carried out using optical measurements and digital image processing techniques. Some experiments from Figueroa-Espinoza and Zenit (2005) were revisited; this particular experimental setup allows for the identification of individual clusters, as well as the measurement of their characteristic parameters, such as size, mean rise velocity, and the added mass effect (mean cluster velocity). Additionally, some statistical properties of the liquid phase such as the mean and fluctuating velocity were obtained using Particle Image Velocimetry (PIV). Particular attention was put on the clusters lifespan, which, by means of a scaling argument based on an analogy to the mean free path of statistical mechanics, was estimated and compared with the measurements as discussed below.

2. Materials and methods

In this investigation two experimental techniques were used: first, bubble position and geometry were obtained by means of a digital high speed camera and image processing, and secondly, the fluid fluctuating velocity was obtained using particle image velocimetry (PIV).

The experimental setup used in this investigation is shown in Fig. 1. A thin channel 20 cm wide and 120 cm high was fabricated with two glass sheets, separated by two glass strips 3 mm thick. Nitrogen millimetric bubbles were produced using an array of 10 identical capillaries, connected to a chamber where pressurized gas was fed through a valve at the channel base. With this array a nearly mono-dispersed stream of bubbles was produced. More details of the experiment can be found in Figueroa-Espinoza and Zenit (2005).

The gas volume fraction α is calculated as follows:

$$\alpha = \frac{V_g}{V_T} = \frac{\Delta H}{H + \Delta H} \tag{6}$$

where V_T and V_g are the total volume of the mixture and the gaseous phase respectively, H is the level of liquid in the channel without bubbles, and ΔH is the increase in height that results from the presence of bubbles. Since the channel is very narrow, a small volume difference causes the level to increase considerably.

Table 1
Fluid properties for different Glycerine percentage in weight at 20 °C. Obtained from tabulated values.

% Weight	ρ(kg/m^3)	$\mu(\times 10^{-3}$Pas)
0 %	9.982	1.005
15%	1.034	1.53
30%	1.073	2.5
50%	1.126	6.0

Mixtures of de-ionized water and glycerine were used in order to vary the liquid properties. In order to reduce coalescence, a small amount of $MgSO_4$ was dissolved in the mixture following Zenit et al. (2001). Since contamination may have an effect on the experiment outcome, the liquid resistivity was monitored: it was always kept larger than 11 MΩ/cm (Table 1).

Experiments were carried out with water, water-glycerine 15% (glyc15 in what follows) and water-glycerine 30% (glyc30). A few tests were also conducted in a water-glycerine 50% mixture (glyc50). The parameter space spanned Reynolds numbers in the range $90 < Re < 600$, and for the Weber number $0.3 < We < 1.6$.

2.1. Digital image analysis

A high speed video camera was used in order to capture images of the bubbly flow at 150 fps. An image processing routine in matlab© was implemented in order to measure the bubbles geometry, as well as their velocity and position. Digital treatment of the images allowed for the identification of clusters: a distance criteria was applied and then neighboring bubbles that complied with this condition were grouped to form individual clusters, as explained in Figueroa-Espinoza and Zenit (2005). In the present study the threshold distance was two pixels in order to measure clusters size more precisely.

It is not obvious how to objectively define a cluster. For practical purposes, we used three criteria: one is the aforementioned distance, the second one is that the bubbles must remain together for some time; only compound objects whose life time was longer than two frames were considered as clusters. The third one is size: a detected object that complies with the previous requisites must be greater than or equal than two average bubble diameters in size to be considered a cluster. Clearly this criteria are arbitrary. Nevertheless, tests for different distances and life times were conducted and the results were not sensitive to the choice of these parameters.

Fig. 2 shows a typical digitally treated image. To the left in (a) the digital image processing routine was used to identify (and label) individual bubbles; to the right (b) individual clusters were identified and labeled, for the same image. The position of their centroids, their area and aspect ratio were recorded, and velocities were calculated using the frame rate of acquisition and calibrated scale images in the horizontal and vertical directions. Note that a dark area without objects is present in the images (at the bottom). This was a mask used to block a region where the back-light was not uniform, in order to avoid false objects detection during the image processing routine.

A routine to identify individual objects in subsequent frames was developed in order to follow trajectories of bubbles and clusters. Clusters were considered to "die" or break when their area (and velocity) changed substantially during one time step. When bubbles separate from the cluster the position of the centroid changes abruptly, and the same thing happens when the cluster leaves the field of view (FOV).

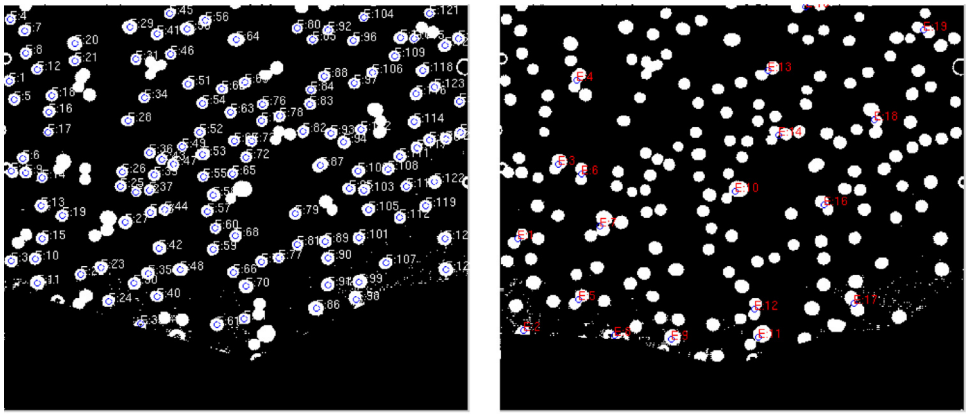

Fig. 2. Binarized image showing detected objects; (a) individual bubbles, (b) clusters. Both views came from the same frame and experiment: water-glycerine 15%, $\alpha = 0.018$.

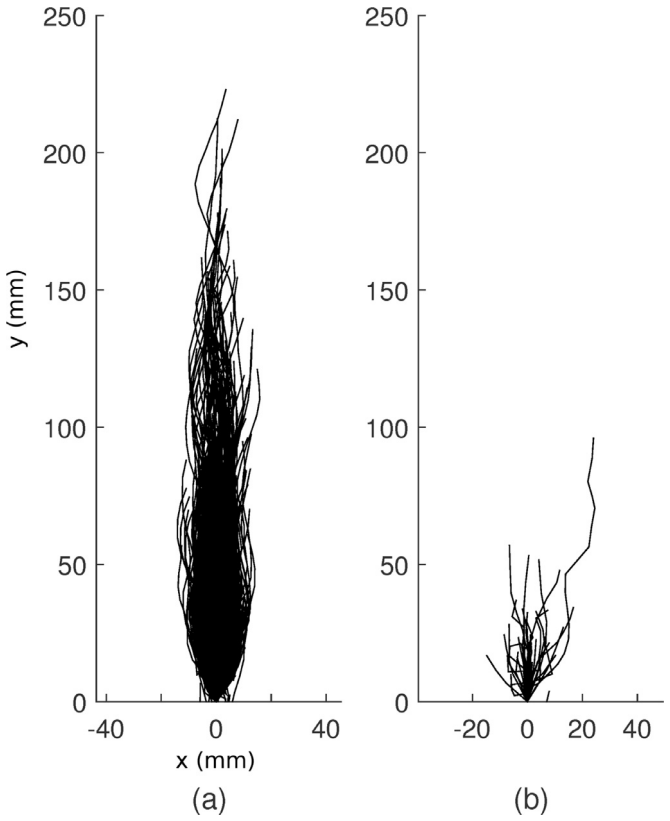

Fig. 3. Trajectories of detected objects through the camera field of view; (a) individual bubbles, (b) clusters for water-glycerine 15%, $\alpha = 0.018$. Axis labels in millimeters.

Fig. 3 shows a set of trajectories, displaced to have the same origin, so the dispersion can be observed as in a bubble plume: to the left in (a) individual bubbles and (b) clusters. It is clear that lifespan of clusters is shorter compared with single bubbles, which can be detected crossing the entire field of view (of about 20 cm × 30 cm). Some individual bubbles have shorter trajectories because some leave the FOV at the borders, and some others are lost because they aggregate forming new clusters.

The uncertainty of these measurements is due to the camera resolution, which is 5.4 pix/mm. Taking into account the frame rate (1/150 s), the error propagates to a maximum value of 2.7 cm/s in the velocity. The error in gas volume fraction is rather small for low α. The maximum uncertainty is estimated to be of $\delta\alpha = 0.0018$, for $\alpha = 0.13$.

2.2. Liquid velocity fluctuations

Liquid velocity fluctuations were obtained using a PIV system capable of measuring the flow field with an acquisition frequency of 10 Hz. The laser sheet (of approximately 0.5 mm thick) was placed at the middle plane between the two glass sheets (channel walls). This is the plane where the dominant components of the motion are located. Fluorescent particles were used as tracers (20 µm diameter, polyamide particles, PSP-20, Dantec Dynamics) in order to reduce reflections from the bubbles surface by using an optical filter. The camera has a 1024 × 1024 pixel sensor. Considering the optical arrange (lens and working distance) the field of view comprised an area of 60 mm × 60 mm approximately, located at equal distances from the channel edges. Therefore, the spacial resolution was 16.7 pixels/mm. To obtain the velocity fields from the PIV images, we used the software Dynamic Studio (Dantec Dynamics). Interrogation areas of 32 × 32 interrogation pixels were considered. Using an adaptive correlation and filtering, the velocity vectors were obtained, comprised of 1024 vectors in each frame. The velocity fluctuations were obtained by averaging in time and space, considering for 600 frames (one minute of measurements). The corresponding results will be discussed in Section 3.1.

The maximum α that could be studied using our setup is relatively large, given the fact that our thin channel allowed for a 2D view of the bubbles (they move confined in a single plane, without overlapping). In our particular case we reached a volume fraction of $\alpha_{max} = 0.13$, the main limitation being the measurement of the mixture height. For larger gas fractions the accumulation of foam at the upper surface yielded imprecise measurements of the increase in height. The maximum uncertainty for α is estimated to be of $\delta\alpha = 0.0018$ for $\alpha = 0.13$).

3. Results

The velocity probability distributions were obtained from a large set of bubbles for each volume fraction as was shown in Figueroa-Espinoza and Zenit (2005). PDF's of the bubble velocity are not shown here for brevity, but they fit normal distributions well, with mean velocities decreasing with α. Fig. 4 shows the mean velocities for all liquids, showing both individual bubbles and clusters. As expected, velocity decreases with volume fraction, and the cluster velocity is always smaller than the velocity of single bubbles, confirming an added mass effect. The dashed line repre-

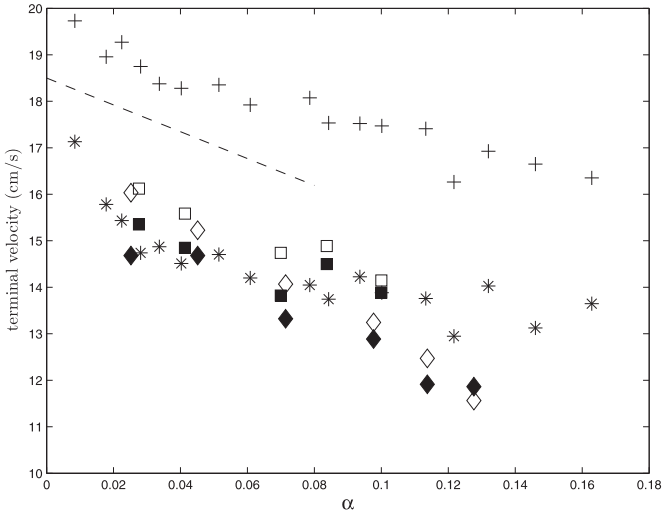

Fig. 4. Bubble and cluster velocity for different values of the gas volume fraction. The markers represent: water bubbles (crosses), water clusters (asterisk), water-glycerine 15% bubbles (empty squares), water-glycerine 15% clusters (filled squares), water-glycerine 30% bubbles (empty diamonds), and water-glycerine 30% clusters (filled diamonds). The dashed line corresponds to Eq. (3).

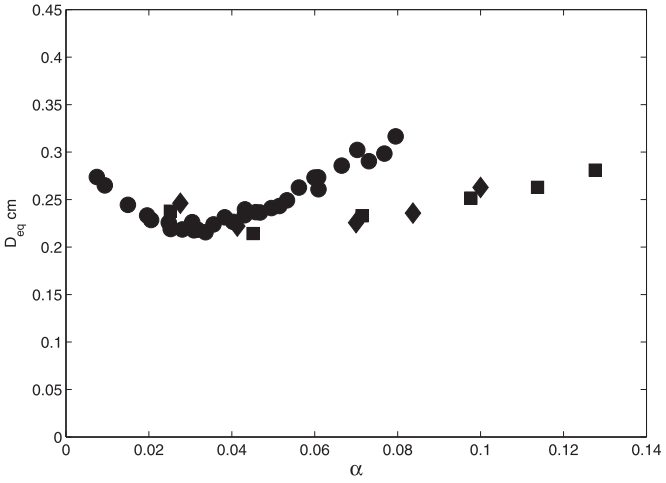

Fig. 5. Equivalent diameter D_{eq} in terms of gas volume fraction α. The different symbols represent tests in different liquids: circles, water; diamonds, glyc15 and squares, glyc30).

sents the theoretical prediction of Van Wijngaarden (1976), given by Eq. (3). Theoretical considerations lead to the correct trend for low bubble fractions, even if the flow is confined between two walls.

It is important to note that the bubble diameter increases with the volume fraction since its formation dynamics changes with the gas flow rate through the capillary tubes. In the experiments reported here the bubble size increased slightly with α, so the bubble diameter was not strictly constant. Fig. 5 shows the equivalent diameter D_{eq} as a function of the gas volume fraction α for different liquids. Various sets of experiments were carried out with different capillaries for injecting the bubbles. They had different lengths and internal diameter. The results presented here were chosen because they presented a smaller growth of D_{eq} with α. Other experiments showed a monotonically increasing D_{eq} with α, with larger variations (more than 56%). The functional relationship $D_{eq}(\alpha)$ is relevant because it will define the behavior of the equivalent Reynolds number, which will be further discussed next. However, the fact that D_{eq} depends on α is not an uncertainty, since the measurement of D_{eq} depends on the number of pixels per millimeter allowed by the optical setup. In our experiments the definition was 5.4 pixels/mm, which represented a maximum uncertainty of approximately 9% for the smallest bubbles (of about $D_{eq} = 2$ mm). The maximum equivalent diameter variations with respect to that of a single bubble (D_{eq} when $\alpha \to 0$) for each liquid was 21% for water, 10% for glyc15 and 18% for glyc30.

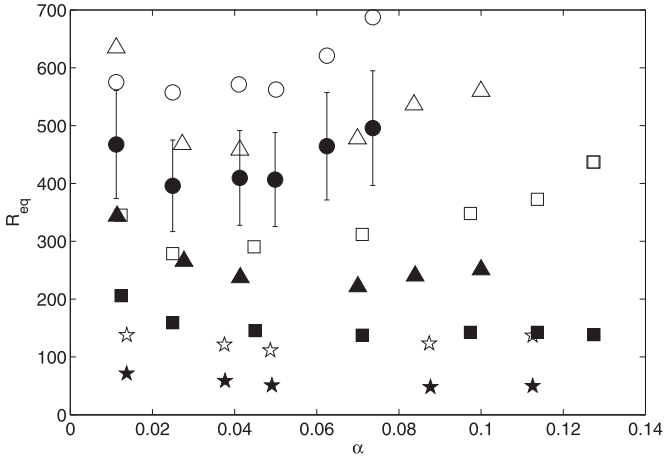

Fig. 6. Equivalent Reynolds number for bubbles and clusters. Filled markers correspond to clusters while empty markers represent bubbles moving in: water (circles), glyc15 (diamonds), glyc30 (squares) and glyc50 (stars).

Bubbles and clusters velocities are also represented in a dimensionless form as an equivalent Reynolds number in terms of the volume fraction α in Fig. 6. This Reynolds number was calculated using the equivalent diameter D_{eq} and the average bubble rise velocity u_b, i.e. $Re_{eq} = u_b D_{eq} \rho / \mu$. The clusters D_{eq} is the equivalent diameter corresponding to a sphere with the same volume as the detected cluster. In the figure, filled markers correspond to clusters while empty markers represent bubbles moving in different liquids: water (circles), glyc15 (diamonds), glyc30 (squares) and glyc50 (stars). The error bars correspond to the propagation of error caused by the uncertainty of D_{eq} and u_b, which in the worst case represents a relative error of approximately 20% in the equivalent Reynolds number.

The equivalent Reynolds number seems to decrease with α for low volume fractions. This appears to be the result of the aforementioned added mass effect. Note that the equivalent Reynolds number should, in principle, follow a monotonically decreasing trend such as that shown in Fig. 3 (for constant viscosity and density). One may observe in Fig. 5 that the way Re_{eq} varies with α follows from the variation of D_{eq} as the gas volume fraction increases.

It is worth noting that clusters always rise slower than individual bubbles for the same conditions. Clusters rise at a slower rate because they are preferably aligned horizontally in this type of experimental setup (Figueroa-Espinoza and Zenit, 2005), which in turn would induce a larger drag coefficient. This is in accordance with Biesheuvel and Van Wijngaarden (1982) who showed that two horizontally aligned bubbles move slower than a bubble pair aligned vertically.

As the volume fraction increases, the mean clusters' area also grows. Fig. 7 shows the clusters mean area A_c, normalized with respect to the mean bubble area A_b for each volume fraction, in a PDF representation. In general, most clusters are formed by two bubbles, and it is less likely to find clusters formed by many bubbles. It can be seen form the figure that for $\alpha = 0.025$ there are fewer clusters formed in the range $3 < A_c/A_b < 4$, while the other two curves ($\alpha = 0.041$ and 0.073) are very similar. The PDF that corresponds to $\alpha = 0.073$ seems to be larger for clusters with areas larger than 5 mean bubble diameters.

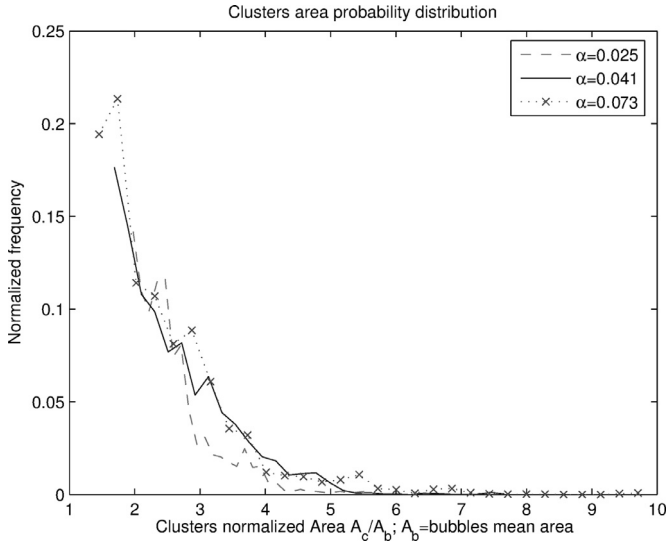

Fig. 7. Probability density function of clusters normalized area with respect to the mean bubble area A_b for water.

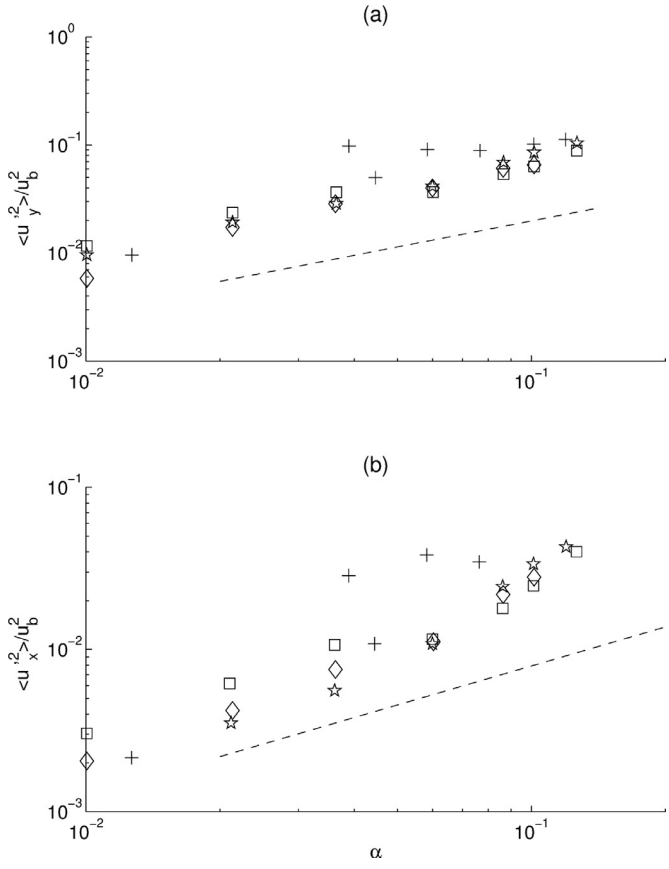

Fig. 8. Normalized liquid velocity fluctuations as a function of gas volume fraction: (a) vertical and (b) horizontal components. Crosses: water, squares: glyc15, diamonds: glyc30, stars: glyc50. The dotted line is a power law proportional to $\alpha^{0.8}$.

Some peaks may appear in the vicinity of $3 < A_c/A_b < 4$ (or more, if α is further increased). The experimental conditions did not allow us to test this tendency for volume fractions higher than 0.13.

Table 2
Power law exponent, m for the vertical liquid velocity fluctuations and 95% confidence intervals (C.I.), *mcorr* stands for the fitted exponent when the fluctuations are normalized with the single bubble velocity $u_b(\alpha \to 0)$.

Liquid	m	C.I.	R^2	*mcorr*	C.I.	R^2 corr
water	0.55	0.02–1.01	0.70	0.38	−024–1.00	0.45
glyc15	0.81	0.45–1.12	0.94	0.51	0.31–0.71	0.93
glyc30	0.90	0.73–1.07	0.99	0.70	0.49–0.91	0.97
glyc50	1.06	0.89–1.23	0.99	0.76	0.63–0.89	0.99

Table 3
Power law exponent for the horizontal liquid velocity fluctuations m and 95% confidence intervals (C.I.), *mcorr* stands for the fitted exponent when the fluctuations are normalized with the single bubble velocity $u_b(\alpha \to 0)$.

Liquid	m	C.I.	R^2	*mcorr*	C.I.	R^2 corr
water	0.99	−0.90–2.90	0.67	0.87	−1.03–2.77	0.60
glyc15	1.38	0.73–2.03	0.92	0.88	0.47–1.29	0.93
glyc30	1.38	0.99–1.76	0.98	1.09	0.81–1.37	0.98
glyc50	1.76	1.41–2.10	0.99	1.39	1.05–1.73	0.98

3.1. Velocity fluctuations

The instantaneous liquid velocity was obtained from the PIV experiments as described in Section 2.2. From these measurements, the mean and standard deviation of the velocity in each direction were obtained, considering variations both in time and space. Fig. 8 shows the normalized liquid vertical velocity fluctuation $< u_y'^2 > /u_b^2$ in (a), as well as the liquid normalized horizontal velocity fluctuation $< u_x'^2 > /u_b^2$ in (b), as a function of gas volume fraction α. Here u_x' and u_y' represent standard deviations of the horizontal and vertical velocity signals. Note that here u_b is not constant, instead, it is the average terminal bubble velocity for the corresponding gas volume fraction α, as described in Mendez et al. (2013) and Martinez-Mercado et al. (2007). The vertical and horizontal velocity fluctuations are much greater than the theoretical lower bound from Eqs. (4) and (5). The dotted line in the figure represents the scaling law $\langle u_y'^2 \rangle / u_b^2 \propto \alpha^m$, where $m = 0.8$. The curves were fitted to the power law and the values of m, the 95% C.I. for m, and R^2 were tabulated on Tables 2 and 3. This power law exponent m for the vertical velocity fluctuations varies between 0.55 (water) and 1.6 (glyc50), which is a similar range as the one in Martinez-Mercado et al. (2007). However our 2D results differ in the sense that in our case the exponent increases as viscosity increases, contrary to the observations in Martinez-Mercado et al. (2007), who observed a decreasing trend with α. For the horizontal liquid velocity fluctuations m goes from 0.99 (water) to 1.76 (glyc50). Note that many authors normalize the velocity fluctuations with the terminal velocity of a single unconfined bubble $u_b(\alpha \to 0)$ (Riboux et al., 2009; 2008; Risso et al., 2008). In order to compare with that normalization, Tables 2 and 3 have columns that show a corresponding exponent for the power law $\langle u_y'^2 \rangle / u_b(\alpha \to 0)^2 \propto \alpha^{mcorr}$, which was estimated from the known variation of the bubble velocity with gas volume fraction. Unfortunately the experimental fluctuations are not conclusive due to the scattering of the data.

The bubbles velocity fluctuations were calculated as well, from the bubbles velocity components u_{bx} and u_{by}. Note that $u_b =< u_{by} >$ and depends on α. Fig. 9 shows the bubble vertical (a) and horizontal (b) bubble normalized velocity fluctuations. Markers represent different liquids. The dotted line shows a power law trend proportional to $\alpha^{0.4}$. These fluctuations behave differently to those of the liquid. The observed exponent for the bubbles case is not in agreement with the one observed in 3D experiments (Riboux et al., 2009). Sangani et al. (1991) studied the problem of a bubble mixture subjected to small-amplitude oscillatory motion. They calculated the normalized variance of the bubbles velocity to

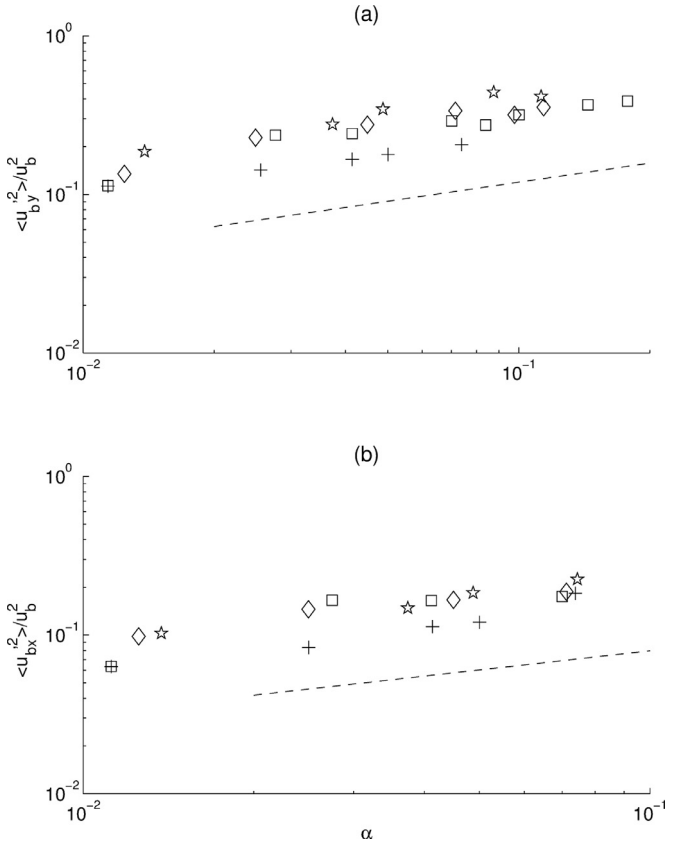

Fig. 9. Normalized bubble velocity fluctuations as a function of gas volume fraction: (a) vertical and (b) horizontal components. Crosses: water, squares: glyc15, diamonds: glyc30, stars: glyc50. The dotted line is a power law proportional to $\alpha^{0.4}$.

Table 4
Power law exponent for the vertical bubble velocity fluctuations m and 95% confidence intervals (C.I.), *mcorr* stands for the fitted exponent when the fluctuations are normalized with the single bubble velocity $u_b(\alpha \to 0)$.

Liquid	m	C.I.	R^2	*mcorr*	C.I.	R^2 corr
water	0.33	0.29–0.36	0.99	0.20	0.16–0.24	0.98
glyc15	0.36	0.25–0.46	0.94	0.10	−0.10–0.30	0.22
glyc30	0.35	0.17–0.53	0.91	0.18	−0.07–0.43	0.67
glyc50	0.39	0.16–0.61	0.93	0.21	−0.08–0.50	0.67

Table 5
Power law exponent for the horizontal bubble velocity fluctuations m and 95% confidence intervals (C.I.), *mcorr* stands for the fitted exponent when the fluctuations are normalized with the single bubble velocity $u_b(\alpha \to 0)$.

Liquid	m	C.I.	R^2	*mcorr*	C.I.	R^2 corr
water	0.65	0.31–0.99	0.94	0.48	0.24–0.62	0.94
glyc15	0.40	−0.40–1.30	0.70	0.31	−0.70–1.31	0.53
glyc30	0.34	0.09–0.59	0.95	0.22	−0.13–0.57	0.80
glyc50	0.49	0.25–0.73	0.98	0.35	0.16–0.53	0.97

leading order in α as:

$$\langle u_{by}'^2 \rangle / u_b^2 = 0.275\alpha \tag{7}$$

The fluctuations obtained experimentally are larger than expected from Eq. (7), and also larger than those reported by Bunner and Tryggvason (2002b) from 3D simulations. It seems that confinement has a strong effect on the bubbles velocity fluctuations. This could be the result of the instability of the trajectory influenced by the walls (Figueroa-Espinoza et al., 2008). The values of the power law exponent m and its goodness of fit are tabulated in Tables 4 and 5, as was explained in previous paragraphs for the case of liquid velocity fluctuations.

3.2. Clusters lifespan

The lifespan of a cluster was considered to be the time lapse between the cluster detection and its breakup (see Section 2.1). Probability density functions were obtained from frequency histograms of the lifespan t_l for each volume fraction α. These lifespan PDFs can be well approximated by log-logistic distributions, commonly used in survival analysis (Kleinbaum and Klein, 2012). Within this context, lifespan (or survival) can be intuitively represented by the Survival Function, which is the complementary cumulative distribution function $SF = 1 - CDF$, where CDF stands for the cumulative distribution function, in terms of lifespan. Clusters lifespan is also shown in nondimensional form, as

$$t_s = t_l u_b / D_{eq}. \tag{8}$$

Hereafter, D_{eq} is the diameter of an equivalent sphere with the same volume as the cluster. We take u_b to be the mean cluster velocity. One point in the *SF* represents the probability of (a cluster) surviving at least t_s. Fig. 10(a) shows an example for $\alpha = 0.062$ as a function of the normalized time t_s. The dotted line is the best fit (log-logistic) SF, and the continuous (stepped) line represents the measured SF from the experimental histogram. To the right, Fig. 10(b) shows the SF functions for three different volume fractions α: solid line: $\alpha = 0.077$, dashed line: $\alpha = 0.062$ and dotted line: $\alpha = 0.054$. As the volume fraction increases, the lifespan decreases.

Fig. 11 shows a plot of timespan as a function of gas volume fraction, for different test liquids, represented with different markers: circles: water, triangles: glyc15, squares: glyc30. Gray and black markers represent different experiments (the gray markers were run with a different bank of capillaries with an internal diameter slightly larger). From this figure it is clear that timespan decreases with volume fraction; however, this trend does not hold for $\alpha < 0.04$. For very low volume fractions, clustering is incipient; most clusters are formed by two bubbles and there are just a few of them. Therefore, in this case the timespan remains unaffected by the change in volume fraction. The uncertainty of the normalized timespan can be estimated using its standard deviation, which decreased with volume fraction; the largest one was about 29% for $\alpha = 0.017$, decreasing to about 16% for $\alpha = 0.12$. We analyzed the propagation of error for the time span of clusters, considering the worst-case scenario in estimating the size of error bars , now shown in Fig. 11. The error may be very large for low α, but reduces to reasonable values for larger α. This uncertainty makes it hard to identify the behavior of the life span for low gas volume fraction. The error propagation for the equivalent Reynolds number turned out to be important, resulting in a 20% variation in the worst case.

The trend (dotted) line represents a power law that scales as $\alpha^{-1.4}$, which will be discussed in the next section.

4. Discussion and conclusions

A nearly monodispersed bubbly flow was studied in a thin channel. Digital image processing routines were used to measure individual bubbles and clusters position, velocity, trajectories, shape and sizes. The added mass effect predicted by potential theory was observed in our thin channel, as a decrease in mean bubble velocity with gas volume fraction α. The trajectories of individual bubbles and clusters were plotted to show the remarkable difference in lifespan between individual bubbles and clusters.

Bubble, clusters and liquid velocity fluctuations were calculated. The latter were obtained using PIV. The normalized liquid (vertical and horizontal) velocity fluctuations for the thin channel are larger than the theoretical prediction given by Eq. (4). The experimental curves for the normalized fluctuations were fitted to a power law

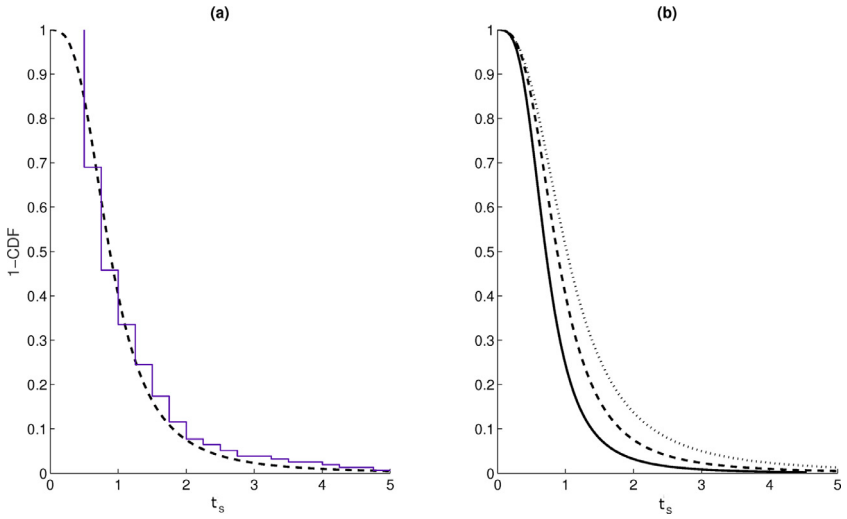

Fig. 10. Survival distribution function in terms of the normalized lifespan. (a) Example for $\alpha = 0.062$. The continuous (stepped) line is a normailzed histogram of the measurements, and the dotted line is the best fit (log-logistic) SF. (b) Shows SF functions for three different volume fractions: solid line: $\alpha = 0.077$, dashed line: $\alpha = 0.062$ and dotted line: $\alpha = 0.054$.

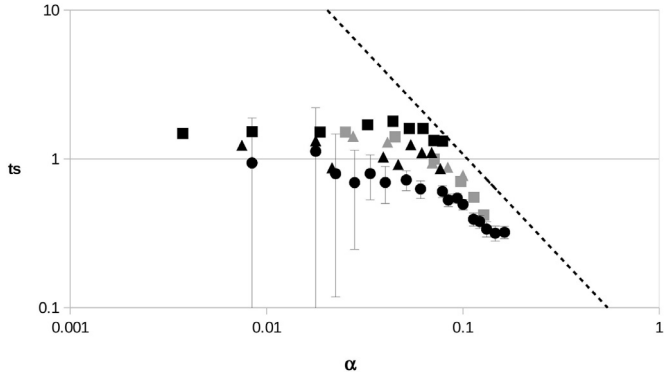

Fig. 11. Clusters normalized lifespan t_s for different volume fractions α, represented with different markers: circles: water, triangles: glyc15, squares: glyc30. Gray and black markers represent different experiments. The trend (dotted) line represents a power law that scales as $\alpha^{-1.4}$.

scaling of the type $\langle u_y'^2 \rangle / U_b^2 \propto \alpha^m$, where m has a value 0.83 for the vertical component of the velocity fluctuations, and 1.38 for the horizontal component. The 95% C.I.s for the power law exponent of the aforementioned scaling accounts for the values reported in the literature (Martinez-Mercado et al., 2007; Mendez et al., 2013; Riboux et al., 2009). Unfortunately the experimental data is scattered and these intervals are still too wide to be conclusive.

The lifetime of clusters was estimated with the individual clusters trajectories through the camera's field of view. This lifetime is dependent on the gas volume fraction α. Experiments show that for very low volume fraction $\alpha < 0.04$ this dependency is very weak, which may result from weak hydrodynamic interactions between the few clusters in the liquid (most of them formed by only two bubbles), at a relative large distance from each other for low α. For larger values of α, the cluster lifespan is greatly reduced.

The mechanism that causes clusters to break can be related to two important factors: bubbles wakes and velocity fluctuations caused by hydrodynamic interactions. Let us consider the latter mechanism in order to find an analogy to statistical mechanics: let us suppose that each cluster will traverse a path, subjected to different hydrodynamic forces (some attractive, that tend to keep the bubbles clustered, and others repulsive or disruptive that tend to break it). Suppose that this trajectory will end, as the mean free path (from statistical mechanics), at a length L, which is defined as:

$$L \propto \frac{1}{\sqrt{2} n \pi D_{eq}^2} \tag{9}$$

where D_{eq} is the cluster equivalent diameter, $n = N/V_T$ is the bubble density number, where N is the number of bubbles. The number density and the gas volume fraction can be related by:

$$\alpha = \frac{V_B}{V_T} = n \frac{\pi}{6} D_{eq}^3 \tag{10}$$

which leads to:

$$L = \frac{D_{eq}}{6\sqrt{2}\alpha}. \tag{11}$$

This length decreases with volume fraction, as expected. If one considers the clusters lifespan t_l to be proportional to L and inversely proportional to the square root of the variance of the velocity:

$$t_l \propto \frac{L}{\sqrt{\langle v_b^2 \rangle}}. \tag{12}$$

And considering that $\langle v_b^2 \rangle$ scales with the volume fraction as:

$$\langle v_b^2 \rangle = k v_b^2 \alpha^q \tag{13}$$

where k is a positive constant of order one, q is an exponent that relates velocity fluctuations to volume fraction ($q = 0.8$ as in Riboux et al., 2009), and v_b is a mean rise velocity , then

$$t_l \propto \frac{D_{eq}}{v_b} \frac{1}{\alpha^{\frac{2+q}{2}}}. \tag{14}$$

For the present case, this leads to:

$$t_s \propto \alpha^{-1.4} \tag{15}$$

which is represented by the dotted line near the normalized lifespan t_s in Fig. 11. This trend is close to the experimental behavior for large α. The slope of the experimental data is not constant, so one cannot draw any quantitative conclusions. One can obtain a fit for the power law for $\alpha > \alpha_s$, for any given threshold α_s, say $\alpha_s = 0.05$, but the choice of this threshold is still arbitrary. The experimental curves were fitted to a power law of the form $t_s \propto \alpha^{-b}$ for the threshold $\alpha_s = 0.05$, and the exponent b, as well as its goodness of fit parameters were tabulated in Table 6. This

Table 6
Power law exponent b for the normalized life span of clusters t_s, 95% confidence intervals (C.I.), and R^2.

liquid	b	C.I.	R^2
glyc15 exp1	−0.54	−1.63–0.55	0.97
glyc30 exp1	−1.34	−1.96–0.72	0.98
water exp2	−0.78	−1.00–0.57	0.90
glyc15 exp2	−0.90	−2.15–0.35	0.83
glyc30 exp2	−0.57	−1.49–0.36	0.78

particular threshold gave fitted values of the power law exponent in the range $-1.34 \leq b \leq -0.54$.

Previous investigations (Bouche et al., 2012) have reported that normalized liquid velocity fluctuations dominated by wake interactions are independent of α, so in that case the resulting exponent would be α^{-1}. Unfortunately it is not clear which is the case, since (depending on the threshold α_s taken) some data are fitted closer to $\alpha^{-1.4}$ and others to α^{-1} (above $\alpha = 0.05$). A more comprehensive experimental campaign could have to be conducted to clarify this issue.

Finally, two regimes were identified in terms of the normalized lifespan: one regime which is independent of α for very low gas volume fraction, and another regime where normalized lifespan decreases as α^{-b}, where according to a scaling argument, the exponent $b = -1$ when the interaction is dominated by wakes, and $b = -1.4$ when hydrodynamic interaction is the main cause of liquid velocity fluctuations. Our results indicate that both mechanisms may be occurring simultaneously.

References

Biesheuvel, A., Van Wijngaarden, L., 1982. The motion of pairs of gas bubble in a perfect liquid. J. Eng. Math. 16, 349–365.
Biesheuvel, A., Van Wijngaarden, L., 1984. Two-phase flow equations for a dilute dispersion of gas bubbles in liquid. J. Fluid Mech. 148, 301–318.
Bouche, E., Roig, V., Risso, F., Billet, A.M., 2012. Homogeneous swarm of high--Reynolds-number bubbles rising within a thin gap. Part 1. Bubble dynamics. J. Fluid Mech. 704, 211–231.
Bunner, B., Tryggvason, G., 2002. Dynamics of homogeneous bubbly flows. Part 1. Rise velocity and microstructure of the bubbles. J. Fluid Mech. 466, 17–52.
Bunner, B., Tryggvason, G., 2002. Dynamics of homogeneous bubbly flows. Part 2. Velocity fluctuations. J. Fluid Mech. 466, 53–84.
Clift, R., Grace, J., Weber, M., 1978. Bubbles, Drops, and Particles. Academic Press.
Eames, I., Hunt, J.C.R., Belcher, S.E., 2004. Inviscid mean flow through and around groups of bodies. J. Fluid Mech. 151, 371–389.
Figueroa-Espinoza, B., Zenit, R., 2005. Clustering in high re monodispersed bubbly flows. Phys. Fluids 17, 091701.
Figueroa-Espinoza, B., Zenit, R., Legendre, D., 2008. The effect of confinement on the motion of a single clean bubble. J. Fluid Mech. 616, 419–443.
Kleinbaum, D.G., Klein, M., 2012. Survival Analysis: A Self Learning Text. Springer.
Kok, J., 1989. Dynamics of Gas Bubbles Moving through Liquid. University of Twente Ph.d. thesis.
Kok, J., 1993. Dynamics of a pair of gas bubbles moving through liquid. Part I. Theory. Eur. J. Mech. Fluids 12, 515–540.
Kumaran, V., Koch, D.L., 1993. The effect of hydrodynamic interactions on the average properties of a bidisperse suspension of high Reynolds number, low Weber number bubbles. Phys. Fluids A 5, 1123–1134.
Kumaran, V., Koch, D.L., 1993. The rate of coalescence in a suspension of high Reynolds number, low Weber number bubbles. Phys. Fluids A 5, 1135–1140.
Lance, M., Bataille, J., 1991. Turbulence in the liquid phase of a uniform bubbly air-water flow. J. Fluid Mech. 222, 95–118.
Martinez-Mercado, J., Palacios-Morales, C.A., Zenit, R., 2007. Measurement of pseudo-turbulence intensity in mono-dispersed bubbly liquids for $10 < \mathrm{Re} < 500$. Phys. Fluids 19, 103302.
Mendez, S., Serrano, J.C., Zenit, R., 2013. Power spectral distributions of pseudo-turbulent bubbly flows. Phys. Fluids 25, 043303.
Mercado, J.M., Prakash, V., Tagawa, Y., Sun, C., Lohse, D., 2013. On bubble clustering and energy spectra in pseudo-turbulence. J. Fluid Mech. 650, 287–306.
Riboux, G., Legendre, D., Risso, F., 2008. A model of bubble-induced turbulence based on large-scale wake interactions. 719 719, 362–387.
Riboux, G., Risso, F., Legendre, D., 2009. Experimental characterization of the agitation generated by bubbles rising at high Reynolds number. J. Fluid Mech. 643, 509–539.
Risso, F., 2011. Theoretical model for k^{-3} spectra in dispersed multiphase flows. Phys. Fluids 23, 011701.
Risso, F., 2016. Physical interpretation of probability density functions of bubble-induced agitation. J. Fluid Mech. 809, 240–263.
Risso, F., 2018. Agitation, mixing, and transfers induced by bubbles. Annu. Rev. Fluid Mech. 50, 25–48.
Risso, F., Amoura, V., Riboux, G., Billet, A., 2008. Wake attenuation in large Reynolds number dispersed two-phase flows. Phil. Trans. R. Soc. Lond. A 366, 2177–2190.
Roig, V., 2007. Measurement of interstitial velocity of homogeneous bubbly flows at low to moderate void fraction. J. Fluid Mech. 572, 87–110.
Salesse, A., Larue de Tournemine, A., Roig, V., 2002. Development of bubble cluster detection and identification method. Exp. Therm Fluid Sci. 26, 163–171.
Sangani, A.S., Didwania, A.K., 1993. Dynamic simulations of flows of bubbly liquids at large Reynolds numbers. J. Fluid Mech. 250, 304–337.
Sangani, A.S., Zhang, D.Z., Prosperetti, A., 1991. The added mass, basset, and viscous drag coefficients in nondilute bubbly liquids undergoing small-amplitude oscillatory motion. Phys. Fluids A 3, 2955–2970.
Smereka, P., 1993. On the motion of bubbles in a periodic box. J. Fluid Mech. 254, 79–112.
Spelt, P., Sangani, A., 1998. Properties and averaged equations for flows of bubbly liquids. App. Sci. Res. 58, 337–386.
Takagi, S., Ogasawara, T., Fukuta, M., Matsumoto, Y., 2009. Surfactant effect on the bubble motions and bubbly flow structures in a vertical channel. Fluid Dyn. Res. 41, 1–17.
Van Wijngaarden, L., 1976. Bubble interactions between bubbles in liquid. J. Fluid Mech. 77, 27–44.
Van Wijngaarden, L., 1993. The mean rise velocity of pairwise-interacting bubbles in liquid. J. Fluid Mech. 251, 55–78.
Van Wijngaarden, L., 1997. On pseudo turbulence. Theor. Comput. Fluid Dyn. 10, 449–458.
Van Wijngaarden, L., 2005. Bubble velocities induced by trailing vortices behind neighbours. J. Fluid Mech. 541, 203–229.
Van Wijngaarden, L., Kapteijn, C., 1990. Concentration waves in dilute bubble/liquid mixtures. J. Fluid Mech. 212, 111–137.
Zenit, R., Koch, D., Sangani, A., 2001. Measurements of the average properties of a suspension of bubbles rising in a vertical channel. J. Fluid Mech. 429, 307–342.